

The behavior of X-ray emission lines from an accretion disk in flare model

A. Róžańska*, B. Czerny*, V. Karas[†], A.-M. Dumont** and S. Collin**

*Copernicus Astronomical Center, Bartycka 18, 00-716 Warsaw, Poland

[†]Academy of Sciences of the Czech Republic, Prague, Czech Republic

**Observatoire de Paris, Section de Meudon, Place Janssen, 92195 Meudon, France

Abstract. We investigate the model of an accretion disk illuminated locally by hard X-rays. The X-ray source is in the form of the hot flares most probably produced via magnetic field reconnection. Flares are accompanied by hot spots created at the accretion disk surface by illumination. We compute the local reflected (spot) spectrum using the codes TITAN/NOAR. In our computations we are able to model the change of intensities of X-ray emission lines from 0.1 keV up to the most prominent iron K_{α} line due to appearance of flares. The global spectrum is obtained assuming a distribution of flares, where each flare has assumed effective life time. In such a case we follow the line profile modified due to relativistic smearing in Kerr metric.

FLARES ABOVE AN ACCRETION DISK

In this paper we present some properties of the X-ray spectra obtained through the modeling of illuminated accretion disk atmosphere in the “flare model”. The main assumption of this model is that during the single flare sudden dissipation occurs in very localized region (coronal loop in close analogy with the solar corona) above the disk surface. In this case the local irradiation flux can be order of magnitude higher than the disk flux itself, but the irradiation is not long lasting and only a small fraction of the disk surface is irradiated at each moment.

Such arrangement of X-ray emitting region has been suggested for the first time by [1], and it was subsequently developed in many papers (e.g. [2]; [3]; [4]; [5]; [6]). The development of a flare leads to a burst of ‘primary emission’ as well as to the formation of a hot spot underlying the flare where roughly half of the X-ray flux is reprocessed by the disk. Irradiation of the disk surface in hydrostatic equilibrium leads to the formation of strongly stratified medium – a hot fully ionized skin covering a cooler, more neutral zone – and so the X-ray spectrum resulting from reprocessing should contain signatures that are characteristic for multi-temperature gas ([7]; [8]; [9]). The irradiating flux is locally very large, exceeding considerably the stationary energy flux which is dissipated inside the disk (e.g. [7]; [8]). The resulting ionized skin is relatively optically thick ([10]).

We are able to follow the individual flare event, and the local reflected spectrum. Our model differs from the so called “lamp post model” in the sense that the region of the disk (illuminated spot) located under the flare

was not illuminated before the flare onset (and in the final state, after the extinction of the flare). After the flare onset, the temperature and the ionization state of the irradiated skin respond immediately to the increase of the continuum, but pressure equilibrium is achieved later. The newly formed hot skin is much denser than an illuminated atmosphere in hydrostatic equilibrium.

Below we briefly describe the parameters of our model and the way of computations of the local reflected spectrum, and we present how equivalent widths of X-ray lines change during one flare.

We also model random distribution of spots and flares across the disk and we account for their motion during the integrated single observation. We consider both non-rotating (Schwarzschild) and rapidly rotating (Kerr) black holes, and we apply general relativity corrections using the KY code of [11].

LOCAL REFLECTED MODEL FOR A SINGLE FLARE .

We model the local spot/flare spectrum as a sum of a flare (primary) emission of a power law shape, and a spot (reflected) emission. The spot emission is determined by using the coupled TITAN/NOAR codes [12] to solve the radiative transfer and the code of [13] to calculate the hydrostatic equilibrium.

Radiative transfer computations were performed for following parameters: the black hole mass of $10^8 M_{\odot}$. The irradiating X-ray flux, $F_X = 10^{15} \text{ erg cm}^{-2} \text{ s}^{-1}$, extends from 1 eV to 100 keV in the form of a power law

TABLE 1. Equivalent widths of most intensive emission lines from the local spot model measured with respect to the reflected continuum, EW_{refl} , and to the sum of the incident plus reflected continuum, EW_{total} . “Hyd” means that lines are computed after hydrostatic equilibrium is achieved while “ion” denotes that only ionization equilibrium is reached.

Ion	Energy [keV]	EW_{refl}^{hyd} [eV]	EW_{total}^{hyd} [eV]	EW_{refl}^{ion} [eV]	EW_{total}^{ion} [eV]
FeXIX	0.118	1.08	0.48	8.62	4.86
CVI $Ly\alpha$	0.367	1.72	0.75	12.3	3.08
NVII $Ly\alpha$	0.500	1.01	0.44	5.95	1.52
OVI - f	0.568	2.59	1.11	27.90	6.86
OVI $Ly\alpha$	0.653	13.32	5.69	104.90	23.15
FeXVII	0.729	2.22	0.94	32.02	7.11
NeX $Ly\alpha$	1.020	4.54	1.91	23.03	5.23
FeXXIV	1.110	4.97	2.07	16.59	3.14
FeXXVI $Ba\alpha$	1.288	2.86	1.18	0.8	0.13
MgXII $Ly\alpha$	1.472	4.50	1.86	18.24	3.73
FeXXIV	1.495	1.48	0.61	4.21	0.86
FeXXVI $Ba\beta$	1.739	1.26	0.51	0.5	0.05
SiXIII - f	1.853	1.23	0.50	25.66	3.87
SiXIV $Ly\alpha$	1.999	12.02	4.95	35.58	6.09
SXV - f	2.446	1.27	0.52	20.95	3.71
SXV $Ly\alpha$	2.611	13.22	5.35	42.58	5.97
FeK α	6.400	1.88	0.76	134.52	28.25
FeXXV - i	6.630	48.69	19.75	45.88	9.63
FeXXV - f	6.667	37.24	15.10	31.67	6.65
FeXXV - f	6.682	49.33	20.00	36.86	7.74
FeXXV - r	6.700	50.07	20.30	39.95	8.39
FeXXVI $Ly\alpha$	6.957	171.9	69.71	40.20	8.44

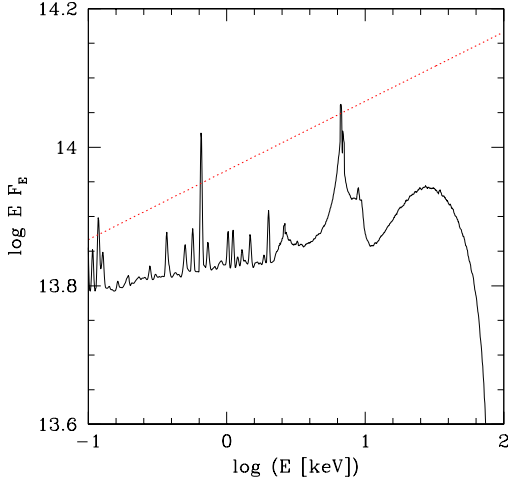


FIGURE 1. Local hot spot reflection spectrum due to irradiation of the disk surface by a flare. Adopted intrinsic spectral resolution $E/\delta E=30$. Dotted line shows the incident spectrum.

(photon index $\Gamma = 1.9$). Iterations between the vertical disk structure (in hydrostatic equilibrium) and radiative transfer are performed till convergence is achieved [9]. We choose the dimensionless accretion rate of 10^{-3} (\dot{m} is scaled to the Eddington rate, $2.2 \times 10^{18} M/M_{\odot} \text{ g s}^{-1}$), and radius $18R_g$ as typical values where local computa-

tions are carried out.

Hence, the ratio of the X-ray incident flux to the disk flux due to the internal dissipation for assumed incident flux and accretion rate is equal to 144. Disk thickness is determined self-consistently by proceeding from the disk surface down to the equatorial plane and adopting the diffusion approximation deeply below the disk atmosphere (for Thomson optical depth ~ 4).

It was shown by [10] that the time scale for ionization equilibrium is much shorter than time scale for hydrostatic equilibrium of illuminated atmosphere. Our computations allow us to follow reflected spectrum through the achievement of ionization equilibrium and then hydrostatic equilibrium.

In Figure 1 we present final intrinsic spectrum of a spot after hydrostatic equilibrium was achieved (i.e. the reflection component). Notice that the disk surface is highly ionized, and so the reflection is efficient also at low energies.

Number of soft X-ray emission lines are visible in spectrum, despite that the adopted irradiation is very strong. Since the soft X-ray emission lines have started to be seen in recent high-quality XMM and Chandra data for AGN ([14]; [15]), we list in Table 1. the equivalent widths of the strongest lines, as measured with respect to the reflected continuum (column 3 and 5) and with respect to total continuum (column 4 and 6). The equivalent widths measured with respect to the total continuum,

i.e. (primary plus reflected) are by a factor of ~ 2.3 lower, as also seen from Fig. 1. In the last two columns of Table 1, the lines are computed after ionization equilibrium was achieved and before hydrostatic equilibrium. Lines after hydrostatic equilibrium are described in column 3 and 4.

The main result of our studying is that the equivalent widths of soft X-ray lines are about five times higher for elements with lower atomic masses (or for lower ionization state see first line of the table) while ionization equilibrium is achieved and before hydrostatic equilibrium. Going toward heavier elements EWs in respect to total continuum become comparable in both cases. Finally, $\text{FeXXV}Ly_{\alpha}$ line is much lower for the case of ionization equilibrium and before hydrostatic one. $K\alpha$ line, in ionization equilibrium only, is about 20 times stronger than after hydrostatic equilibrium is obtained. This fact may be important while we want to follow the change of line flux in time.

FLARE/SPOT DISTRIBUTION ABOVE THE WHOLE DISK

In the next step we consider flare distribution over whole accretion disk. Irradiated hot spots move with the disk around the central black hole and eventually decay while new spots continuously emerge.

Fundamental parameters of the model are the mass of the black hole, M , and the mean X-ray luminosity, L_X . This X-ray luminosity is assumed to originate from n_{mean} flares per second, on average. The actual number of flares fluctuates at any given moment around this mean value according to Poisson's distribution. Flares are assumed to corotate with the underlying disk.

A fraction of radiation from each flare reaches the observer as the direct component. On the other hand, part of flare photons are reprocessed by the disk surface and it produces the reflection component. Full model is presented in the paper [16].

GENERAL RELATIVITY EFFECTS IN PREDICTED SPECTRA

Thanks to its featureless power-law character, relativistic effects do not affect the spectral shape of primary continuum emission. However, spectral lines are still subject to the well-known relativistic smearing ([17]; [18]). It is interesting to see if the smearing of a realistic spectrum is distinguishable from the case of separate monochromatic lines which may be superimposed on broad-band continuum.

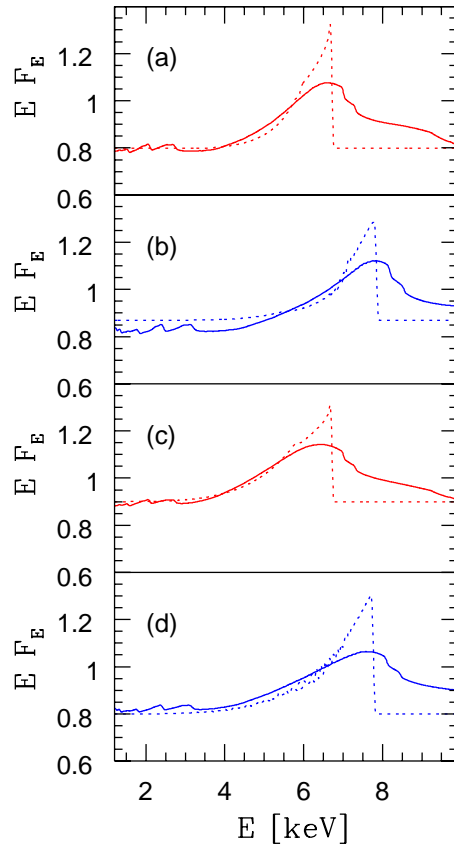


FIGURE 2. The reflection spectrum from the disk uniformly covered with spot-like emission and the local emissivity decreasing as r^{-3} up to $R_{\text{out}} = 50R_g$. The case of Schwarzschild black hole, $a = 0$, inclination 30° (panel a), $a = 0$, inclination 60° (panel b), rapidly rotating Kerr $a = 0.998$, inclination 30° (panel c), and $a = 0.998$, inclination 60° . Dotted lines show the case of relativistically smeared monochromatic line at 6.4 keV superimposed on a flat continuum.

To examine the effect of the smearing we consider the disk surface, which is covered uniformly by a spot-like emission. The local emissivity is given by the reflection component, as specified in the second section. The emissivity is assumed to decrease with the disk radius as r^{-3} .

There is clear distinction between the relativistic smearing of a monochromatic line and the shape of the relativistically smeared realistic reflection component.

In order to include general relativity effects in the Kerr spacetime, we have developed a new computational routine which combines advantages of different approaches used in the past ([18]; [19]; [20]). A redesign was desirable in order to achieve sufficient resolution in both energy and time for the signal arising in multiple spots that are spread over the whole range of radii. The routine,

KY, is flexible enough to allow easy modifications of local emissivity profiles and it can be used as a rapid standalone code as well as linked to the standard XSPEC package ([21]) for X-ray spectral analysis. In this paper we linked KY with the above-described computations of intrinsic emissivity of the spotted disk. For further details see [11].

The influence of relativistic corrections on the local spectrum can be parameterized by the angular momentum of the black hole, a , and the inclination angle of an observer, i . On the other hand, by scaling lengths with R_g and time intervals with R_g/c , one conveniently ensures that graphs of predicted spectra do not explicitly show dependence on the black hole mass.

From Figure 2 we see that the sharp blue edge, which is characteristic for a monochromatic line, is replaced by much smoother feature. This is due to the presence of double-peaked and Compton-broadened $K\alpha$ line in the realistic spectrum, as well as due to the contribution of $K\beta$ and the Compton-smearing iron edge.

Weak emission lines of other elements are also noticeable in smeared spectra. Therefore it is not surprising that traces of these relativistically broadened emission lines are noticeable in the observational data (e.g. [14] for NGC 5548 and [15] for Ton S180). Soft X-ray lines as strong as those claimed to be detected in the data by [22] and [23] are not expected within the frame of our model.

This result clearly supports the argument ([24]; [25]; [26]; [27]; [28]; [29]) that proper interpretation of the observational data requires consideration of the relativistic broadening of the entire reflected component, i.e. the reflected continuum together with the iron line, instead of treating the two components separately.

ACKNOWLEDGMENTS

This work was supported by grant 2P03D00322 of the Polish State Committee for Scientific Research and by Jumelage/CNRS No. 16 "Astronomie France/Pologne". VK acknowledge support from grants GAUK 188/2001 and GACR 205/03/0902.

REFERENCES

- Galeev A. A., Rosner R., Vaiana G. S., 1979, ApJ, 229, 318
- Abramowicz M. A., Bao G., Lanza A., Zhang X.-H., 1991, A&A, 245, 454
- Haardt F., Maraschi L., Ghisellini G., 1994, ApJ, 432, 95
- van Oss R. F., van den Oord G. H. J., Kuperus M., 1993, A&A, 270, 275
- Poutanen J., Fabian A.C., 1999, MNRAS, 306, L31
- Życki P. T., 2002, MNRAS, 333, 800
- Nayakshin S., Kazanas D., Kallman T. R., 2000, ApJ, 537, 833
- Ballantyne D. R., Ross R. R., Fabian A. C., 2001, MNRAS, 327, 10
- Różańska A., Dumont A.-M., Czerny B., Collin S., 2002, MNRAS, 332, 799
- Collin S., Coupé, S., Dumont, A.-M., Petrucci, P.-O., Różańska, A., 2003, A&A, 400, 437
- Dovčiak M., Karas V., Yaqoob T., 2003, in *Proc. of the Workshop on Processes in the Vicinity of Black Holes and Neutron Stars*; October 2003, Opava. Eds. S. Hledí & Z. Stuchlík, submitted
- Dumont A.-M., Abrassart A., Collin S., 2000, A&A, 357, 823
- Różańska A., Czerny B., Życki P.T., Pojmański G., 1999, MNRAS, 305, 481
- Kaastra J.S., Steenbrugge K.C., Raassen A.J.J., van der Meer, R.L.J., Brinkman A.C., Liedahl D.A., Behar E., de Rosa A., 2002, A&A, 386, 427
- Różańska A., Czerny B., Siemiginowska A., Dumont A.-M., Kawaguchi T., 2003, Apj (in press), astro-ph/0309430
- Czerny, B., Różańska A., Dovčiak M., Karas V., Dumont A.-M., 2004, A&A, (submitted)
- Fabian A.C., Rees M.J., Stella L., White N.E. 1989, MNRAS, 238, 729
- Laor A., 1991, ApJ, 376, 90
- Karas V., Vokrouhlický D., Polnarev A. G., 1992, MNRAS, 259, 569
- Martocchia A., Matt G., Karas V., 2002, A&A, 383, L23
- Arnaud K. A., 1996, in *Astronomical Data Analysis Software and Systems V*. Eds. Jacoby G. & Barnes J.; ASP Conf. Series, vol. 101, p. 17
- Branduardi-Raymont G., Sako M., Kahn S. M., Brinkman A. C., Kaastra J. S., et al., 2001, A&A, 365, L140
- Mason K. O., Branduardi-Raymont G., Ogle P. M., Page M. J., Puchnarewicz E. M., et al., 2003, ApJ, 582, 95
- Życki P. T., Done C., Smith D. A., 1997, ApJ, 488, L113
- Bao G., Wiita P. J., Hadrava P., 1998, ApJ, 504, 58
- Young A.J., Ross R.R., Fabian A.C., 1998, MNRAS, 306, 461
- Martocchia A., Matt G., Karas V., 2002, A&A, 383, L23
- Gondoin P., Orr A., Lumb D., Santos-Lleo M., 2002, A&A, 388, 74
- Ballantyne D. R., Vaughan S., Fabian A. C., 2003, MNRAS, 342, 239